Research Article Vol. 12, No. 9 / 1 Sep 2021 / Biomedical Optics Express 5499
Biomedical Optics EXPRESS

Dec-DISCO: decolorization DISCO clearing for seeing through the biological architectures of heme-rich organs

JINGTAN ZHU,[1,2] YILIN MA,[1,2] JIANYI XU,[1,2] YUSHA LI,[1,2] PENG WAN,[1,2] YISONG QI,[1,2] TINGTING YU,[1,2,*] AND DAN ZHU[1,2]

[1]*Britton Chance Center for Biomedical Photonics, Wuhan National Laboratory for Optoelectronics, Huazhong University of Science and Technology, Wuhan, Hubei 430074, China*
[2]*MoE Key Laboratory for Biomedical Photonics, School of Engineering Sciences, Huazhong University of Science and Technology, Wuhan, Hubei 430074, China*
[*]*yutingting@hust.edu.cn*

Abstract: The tissue optical clearing technique plays an important role in three-dimensional (3D) visualization of large tissues. As a typical solvent-based clearing method, 3DISCO can achieve the highest level of tissue transparency with favorable clearing speed. However, 3DISCO cannot deal with the residual blood within tissues, leading to tissue brownness or redness after clearing, thus greatly influencing the tissue transparency and image quality due to the strong absorption of residual blood. To address this problem, we proposed an optimized clearing method by introducing CUBIC-L solution combined with 3DISCO for effective decolorization, termed Dec-DISCO (Decolorization DISCO). Dec-DISCO achieves better transparency than 3DISCO for various heme-rich tissues and performs enhanced fluorescence preservation capability. Dec-DISCO allows high-quality 3D imaging of fluorescently labeled heme-rich organs, as well as pathological tissue with severe hemorrhage. Dec-DISCO is expected to provide a powerful tool for histological analysis of kinds of heme-rich tissues in various medical conditions.

1. Introduction

Accurate mapping of tissue structures in three-dimension can significantly promote the understanding of the overall complex biological architectures and functions for whole organs and organisms [1–5]. Recently, 3D imaging with high resolution benefits from the rapid development of optical imaging techniques and fluorescent labeling techniques [6,7]. However, the high light scattering within tissues limits the imaging depth of optical tomography [8]. The advent of modern tissue optical clearing techniques efficiently reduces the light scattering and renders the tissue highly transparent, deepening the optical imaging depth and provides a powerful tool for 3D reconstruction of the intact organs [9,10].

In recent years, various tissue clearing methods have been developed. They are principally divided into three groups: solvent-based methods, such as 3DISCO [11,12], iDISCO [13], uDISCO [14], FDISCO [15], vDISCO [16], sDISCO [17] and PEGASOS [18], aqueous-based methods, such as SeeDB [19,20], Sca*l*eS [21], FOCM [22], MACS [23] and CUBIC [24–26], and hydrogel-based methods, such as CLARITY [27,28], PACT [29] and SHIELD [30]. Aqueous-based methods and hydrogel-based methods are known for high levels of fluorescence compatibility and well preservation of tissue morphology, but are limited by long clearing time or insufficient transparency [9]. In contrast, organic solvent-based clearing protocols, such as 3DISCO, can achieve the highest level of tissue transparency with favorable clearing speed. Therefore, 3DISCO is widely used for imaging large samples, such as brains, spinal cords, muscles, embryos, and so on [31–35]. However, 3DISCO cannot deal with the residual blood within tissues, causing tissue brownish or redness after clearing [14,15,36]. Though careful

#431397 https://doi.org/10.1364/BOE.431397
Journal © 2021 Received 14 May 2021; revised 11 Jul 2021; accepted 2 Aug 2021; published 11 Aug 2021

Biomedical Optics EXPRESS

intracardial perfusion with PBS was done prior to tissue extraction, some tissues still contained substantial residual blood, such as liver, kidney, spleen, and lung, which significantly affected the tissue transparency and imaging quality after clearing. This blood-sensitive feature greatly affected the applications of 3DISCO in studying heme-rich tissues for health and disease.

In this study, we aim to modify 3DISCO method by introducing an effective decolorization solution prior to 3DISCO clearing. We screened many kinds of chemicals used for decolorization and found that CUBIC-L was efficient for decolorization and also preserved fluorescence well. We therefore combined 3DISCO with CUBIC-L pretreatment, and this whole pipeline was termed as Dec-DISCO (Decolorization DISCO). Dec-DISCO enables efficient decolorization and clearing of heme-rich rodent organs with stabilized fluorescence preservation. With Dec-DISCO, we achieved high-quality imaging for neural structures of adult mouse brains and muscles with transgenic labels, and performed complete imaging of mouse lungs without blind areas labeled by quantum dots. We also used Dec-DISCO to visualize the neural disruptions in the injured spinal cord with severe hemorrhage. These results suggest that Dec-DISCO protocol provides an efficient alternative for clearing and imaging of heme-rich tissues and is expected to be used for 3D visualization of various tissues for health and disease.

2. Materials and methods

2.1. Animals

Wild-type (C57BL/6J) (8–11 weeks old), *Thy1*-GFP-M (8–11 weeks old), *Thy1*-YFP-16 mice (8–11 weeks old), and Sprague-Dawley rats (200–250 g) were used in this study. Animals were selected for each experiment based on their genetic background (wild-type or fluorescence transgenes). All animal care and all experimental procedures followed the Experimental Animal Management Ordinance of Hubei Province, P. R. China and the guidelines from the Huazhong University of Science and Technology, and were approved by the Institutional Animal Ethics Committee of Huazhong University of Science and Technology.

2.2. Preparation of samples

Mice and rats were deeply anesthetized with a mixture of 2% α-chloralose and 10% urethane (8 mL/kg) through intraperitoneal injection, and perfused intracardially with 0.01 M phosphate buffered saline (PBS) (Sigma-Aldrich, St. Louis, USA) followed by 4% paraformaldehyde (PFA) (Sigma-Aldrich, St. Louis, USA) in PBS. After perfusion, tissues of interest (brain, heart, liver, spleen, lung, kidney, and muscle) were carefully dissected from the perfused mouse body and post-fixed in 4% PFA overnight at 4 °C. The brain samples used in Fig. 3 were directly extracted from the sacrificed mice without perfusion followed by fixation in 4% PFA overnight at 4 °C. All organs were rinsed with PBS several times. 1-mm-thick coronal brain slices were obtained using a commercial vibratome (Leica VT1200S, Germany).

2.3. Preparation of decolorization solutions

8% sodium dodecyl sulfate (SDS) was prepared by dissolving SDS powder (30166428, Sinopharm Chemical Reagent Co. Ltd., China) in distilled water at a concentration of 8% (wt/vol). 0.1 M NaOH was prepared by dissolving NaOH powder (10019718, Sinopharm Chemical Reagent Co. Ltd., China) in distilled water at the indicated concentration. 5% H_2O_2 was prepared by diluting 30% H_2O_2 stock solution (80070961, Sinopharm Chemical Reagent Co. Ltd., China) with distilled water. CUBIC-R1 was prepared as a mixture of 25 wt% N,N,N',N'-tetrakis(2-hydroxypropyl) ethylenediamine (T0781, Tokyo Chemical Industry, Japan), 25 wt% urea (10023218, Sinopharm Chemical Reagent Co., Ltd, China) and 15 wt% Triton X-100 (10789704001, Sigma-Aldrich, USA) dissolved in distilled water, as previously reported [24]. CUBIC-L was prepared as a

Biomedical Optics EXPRESS

mixture of 10 wt% Triton X-100 and 10 wt% N-buthyldiethanolamine (B0725, Tokyo Chemical Industry, Japan) dissolved in distilled water, as previously reported [26].

2.4. Dec-DISCO clearing procedure

Fixed samples were firstly immersed in CUBIC-L solution for decolorization for 1–3 d, the time needed for this step depends on the sample size. The decolorized samples were then washed with PBS several times. Then the samples were incubated successively in increasing tetrahydrofuran (THF) (186562, Sigma-Aldrich) concentrations (50 vol%, 70 vol%, 80 vol%, 100 vol%, 100 vol%) for dehydration, followed by incubation in dibenzyl ether (DBE) (108014, Sigma-Aldrich) for refractive index (RI) matching. All steps were performed at room temperature with gentle shaking. The time needed for clearing is 1-12 h for each dehydration step, and 1-3 h for RI matching, which depends on tissue thickness.

2.5. Measurement of light transmittance

We measured the light transmittance of whole mouse kidneys using a commercially available spectrophotometer (Lambda 950, PerkinElmer, USA). Cleared samples were mounted in a cuvette fulfilled with RI matching solution for measurement of transmittance. We measured transmittance spectra from 400 nm to 800 nm. Each sample was measured three times independently, and data for plotting was based on the average value.

2.6. Quantum dot labeling

The fluorescent quantum dots used in this study are based on zinc sulfide quantum dots coated with cadmium selenide (CdSe@ZnS 488). The quantum dots are firstly embellished by Glutathione (GSH) to transform it from the hydrophobic organic state into a more biocompatible water-miscible state. Subsequently, the mice (C57BL/6J) were anesthetized, followed by injection of 400 μL quantum dots through the tail vein to complete the labeling. Following successful injections, animals recovered from anesthesia in a warm cage for about 30 min, then returned to their home cage. The labeled mice were sacrificed 6 h after injection.

2.7. Spinal cord injury model

Mice (C57BL/6J) were deeply anesthetized and placed on a heating pad (37°C) to maintain body temperature during surgery. The back skin was incised, and the muscle tissue was then dissected to expose laminae T9 to T11. A T10 laminectomy was completed by removing the dorsal lamina carefully. Contusive thoracic (T10) spinal cord injury (SCI) was induced using a blunt force impactor (modified NYU device), as described in previous literature [37]. After injury, the muscle and skin were carefully sutured. The mice were then placed in a warm cage with soft padding and maintained at 37 °C until fully awake.

2.8. Imaging

Fluorescence images of cleared samples (adult mouse brains, spinal cords, and lungs) were acquired with a light sheet microscope (Ultramicroscope I, LaVision BioTec, Germany) equipped with a sCMOS camera (Andor Neo 5.5, Oxford Instrument, UK), a macrozoom body (MVX-ZB10, Olympus, Japan, magnification from 0.63× to 6.3×) with a 2× objective lens (MVPLAPO2X, Olympus, Japan, NA = 0.5, WD = 20 mm), and a dipping cap. Thin light sheets were illuminated from both the right and left sides of the samples. We acquired light-sheet microscope stacks using ImSpector (Version 4.0.360, LaVision BioTec, Germany) as 16-bit grayscale TIFF images for each channel with a 5 μm step size.

An inverted laser-scanning confocal fluorescence microscope (LSM710, Zeiss, Germany) was used to perform fluorescence imaging of brain slices. Samples were placed on a slide and

Biomedical Optics EXPRESS

covered with a coverslip to keep tissue submerged in clearing solutions. A 5× objective lens (FLUAR, NA=0.25, WD=12.5 mm), 10× objective lens (FLUAR, NA=0.5, WD=2 mm), and a 20× objective lens (PLAN-APOCHROMAT, NA=0.8, WD=550 μm) were used for imaging.

2.9. Data processing

All raw image data were collected in a lossless TIFF format (8-bit for confocal microscopy and 16-bit for light sheet microscopy). Processing and 3D rendering were executed by a Dell workstation with 16 core Xeon processor, 256 GB RAM, and Nvidia Quadro P2000 graphics card. We used Imaris (Version 7.6, Bitplane AG) and Fiji (Version 1.51n) for 3D and 2D image visualization, respectively. Stitching of tile scans from light sheet microscopy was performed via Matlab (Version 2014a, Mathworks). The 16-bit images were transformed to 8-bit images with Fiji to enable fast processing using different softwares.

2.10. Quantifications

Measurement of tissue size changes. 1-mm-thick brain slices were used for the measurement of sample expansion and shrinkage, and bright-field images were taken before and after clearing. The coronal area of the sample was determined using the 'polygon-selections' function of Fiji. The tissue size change was determined by calculating the ratio of the area before and after clearing (Fig. S4b).

Relative fluorescence quantification. For evaluation of relative fluorescence intensity, the cell body of a neuron was encircled by the 'freehand-selection' tool in Fiji, then the mean fluorescence intensity and area were measured. The multiplication values of these two parameters were identified as the total fluorescence intensity of the neurons. The total fluorescence intensity was normalized to the value in PBS (100%) for the same neuron, which was defined as relative fluorescence intensity (Fig. 1(e), 1(f); Fig. S1b; Fig. S2b). For quantification of light sheet imaging data, we used a well-established pipeline previously reported in Ref. [15] (Fig. 3(h)).

2.11. Statistical analysis

Data are presented as the mean ± SD. and were analysed using SPSS software (Version 22, IBM, USA) with 95% confidence interval. Sample sizes are indicated in the figure legends. For analysis of statistical significance, the normality of the data distribution in each experiment was checked using the Shapiro-Wilk test. The variance homogeneity for each group was evaluated by Levene's test. P values were calculated using an independent-sample t-test (two-sided) to compare data between two groups in Fig. 3(h), Fig. S2b, and Fig. S4b. P values were calculated using one-way ANOVA followed by the Bonferroni post hoc test to compare data in Fig. 1(e), Fig. 1(f), and Fig. S1b. In this study, $P < 0.05$ was considered significant (*, $P < 0.05$; **, $P < 0.01$; ***, $P < 0.001$).

Biomedical Optics EXPRESS

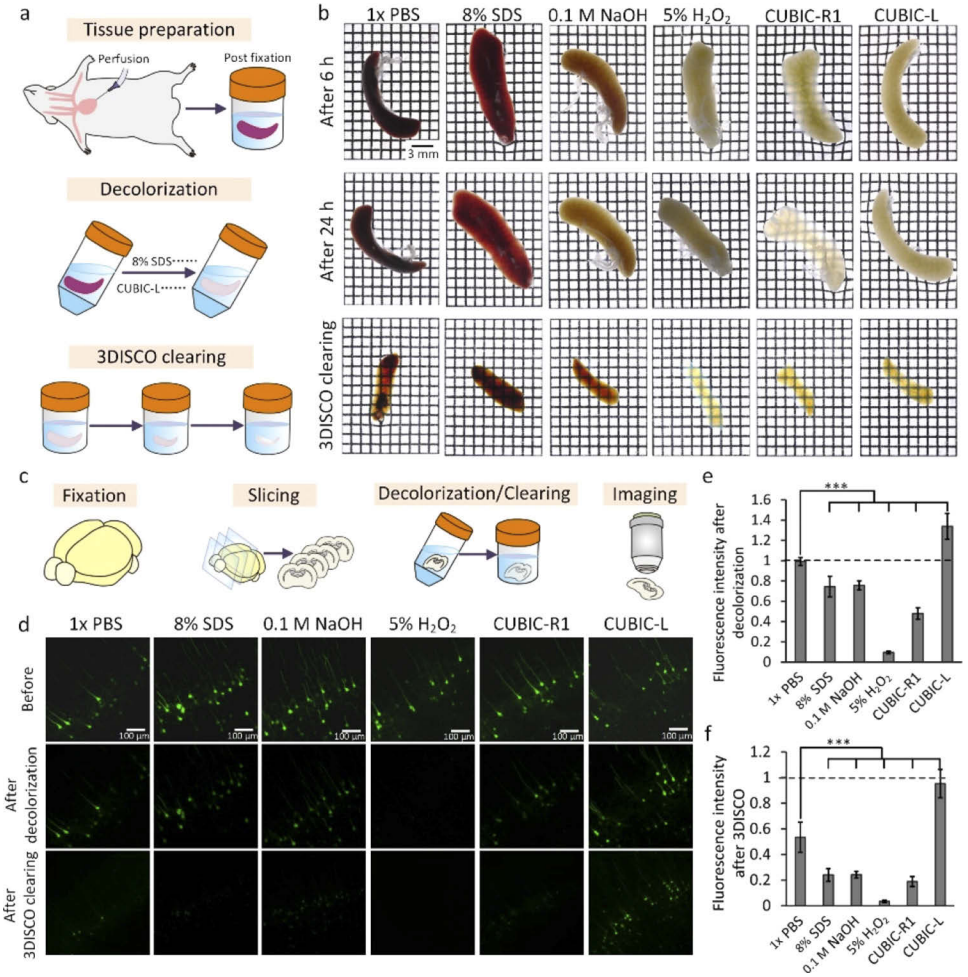

Fig. 1. Modifying 3DISCO by tissue decolorization. (a) Work flow for evaluating the decolorization abilities for chosen solutions. (b) Bright-field images of adult mouse spleens treated by different decolorization reagents. (c) Experimental pipeline for quantifying the fluorescence preservation abilities for different decolorization solutions. (d) Fluorescence images of mouse brain slices after decolorization by indicated solution and after 3DISCO clearing. All confocal images are MIPs of z stacks (50 μm thick) from the surface. (e) Comparison of fluorescence intensity of brain samples after decolorization by different reagents prior to clearing (n=6). (f) Comparison of fluorescence intensity of decolorized samples after 3DISCO clearing (n=6). All values are presented as the mean ± SD. Statistical signifcance in **e** and **f** (***, $P < 0.001$) was assessed by one-way ANOVA followed by the Bonferroni post hoc test.

Biomedical Optics EXPRESS

3. Results

3.1. Modifying 3DISCO by decolorization with enhanced endogenous fluorescence intensity

3DISCO clearing method is significantly effective for 3D imaging of large volumes, owing to its superior clearing capabilities, and has been widely used in many biomedical studies. However, 3DISCO method cannot deal with the residual blood within tissue, thus the samples cleared by 3DISCO often display a deep red color, especially for heme-rich tissue. The residual blood within cleared tissue will lead to severe light absorption in the visible region (400–600 nm), affecting tissue transparency and imaging quality. Therefore, we tried to introduce efficient decolorization solutions to address this issue for 3DISCO method. We selected several typical solutions for tissue decolorization, including 8% SDS, 0.1 M NaOH, 5% H_2O_2, CUBIC-R1, and CUBIC-L. We used fixed mouse spleens with plenty of residual blood to examine the decolorization abilities of these solutions, as well as compatibilities with 3DISCO clearing (Fig. 1(a)). We found that 5% H_2O_2, CUBIC-R1, and CUBIC-L successfully decolorize mouse spleens within 24 h, leading to high transparency after 3DISCO clearing (Fig. 1(b)).

In addition to tissue transparency, the compatibilities of the above solutions with endogenous green fluorescent proteins (GFP) were also investigated (Fig. 1(c)). The tested 8% SDS, 0.1 M NaOH, 5% H_2O_2, and CUBIC-R1 solutions all attenuated GFP signals to different degrees after decolorization. However, the fluorescence intensity of GFP signals increased obviously after decolorization by CUBIC-L (Fig. 1(d, e)). This fluorescence enhancement by CUBIC-L could retain considerable GFP signals even after the subsequent 3DISCO clearing, which could not be achieved by other tested solutions (Fig. 1(d, f)). We also found that N-butyldiethanolamine used in CUBIC-L lead to the enhancement of GFP fluorescence, probably due to its alkaline condition in water (Fig. S1). Taking both transparency and fluorescence preservation into consideration, we chose CUBIC-L for decolorization prior to clearing, and the entire pipeline was termed as Dec-DISCO (Decolorization 3DISCO) (Fig. 2(a)). Additionally, we also compared the fluorescence preservation between Dec-DISCO protocol and the original CUBIC protocol. The results suggested that Dec-DISCO protocol showed much better fluorescence preservation than CUBIC protocol after complete clearing (Fig. S2).

3.2. Dec-DISCO allows sufficient clearing for heme-rich rodent organs

Firstly, we compared the clearing performance between Dec-DISCO and original 3DISCO on adult mouse organs with heavy residual blood. As shown in Fig. 2(b), Dec-DISCO successfully eluted the heme chromophore within mouse kidneys and showed better clearing performance than 3DISCO. The transmittance curves also demonstrated that compared with 3DISCO, Dec-DISCO significantly improved the tissue transparency, especially in the visible range between 400 to 600 nm (Fig. 2(c)). Dec-DISCO was also more effective on other types of rodent organs than 3DISCO, such as rat organs (Fig. 2(d)). Additionally, we also cleared the rat organs with the original CUBIC protocol. Dec-DISCO protocol could achieve high transparency of rat organs within 7 d, however, a 10 d protocol was not enough for CUBIC to achieve complete transparency on typical rat organs, such as heart, spleen, and kidney (Fig. S3).

The feature of tissue shrinkage achieved by 3DISCO is beneficial for imaging large-volume tissues, for it can help reduce the acquisition time and shorten the requirement for work distance of objectives needed for imaging. Therefore, we also measured the size change of tissue cleared by Dec-DISCO and 3DISCO. 1-mm-thick brain slices were cleared by Dec-DISCO and 3DISCO, respectively. Bright-field images were taken, and the outlines of samples were traced before and after clearing. The traced border of brain sections showed similar outlines before and after clearing for both two methods, while the quantified tissue shrinkage achieved by Dec-DISCO showed slightly larger than 3DISCO (Fig. S4).

Biomedical Optics EXPRESS

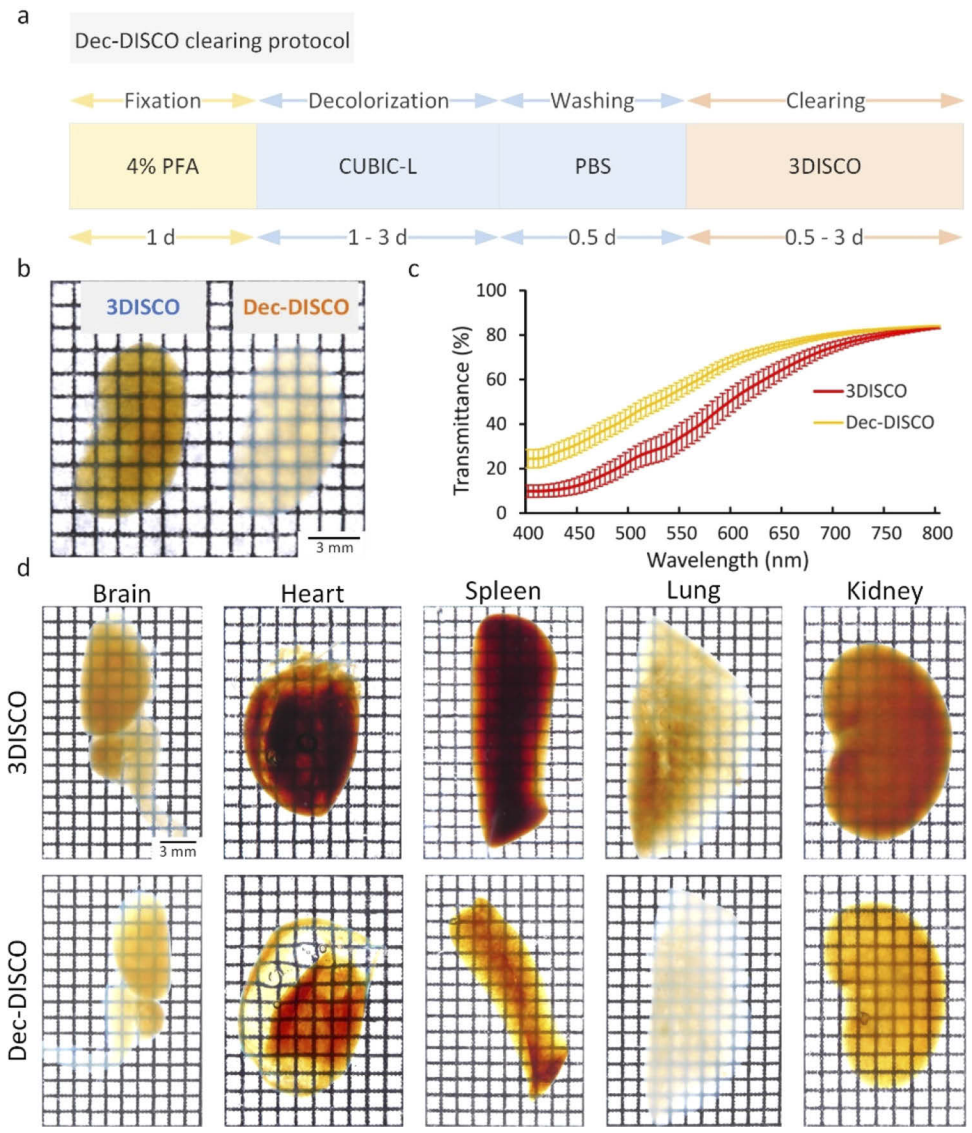

Fig. 2. Dec-DISCO allows high-performance clearing for heme-rich rodent tissues. (a) The entire pipeline for Dec-DISCO clearing. (b) Bright-field images of adult mouse kidneys cleared by 3DISCO and Dec-DISCO, respectively. (c) Transmittance curves of adult mouse kidneys cleared by 3DISCO and Dec-DISCO (n = 3). (d) Bright-field images of different rat organs cleared by 3DISCO and Dec-DISCO. All values are presented as the mean ± SD.

Biomedical Optics EXPRESS

3.3. Dec-DISCO permits high-quality imaging for adult mouse tissue using LSFM

To investigate the superiority of Dec-DISCO over 3DISCO in 3D imaging, we compared the imaging quality of Dec-DISCO with 3DISCO using adult *Thy1*-GFP-M mouse brains expressing endogenous GFP signals. We divided a *Thy1*-GFP-M mouse brain without perfusion into two halves, one for Dec-DISCO and the other for 3DISCO, and imaged them using light sheet illuminated from the same side (Fig. 3(a)). Figure 3(b) showed the bright-field images before and after clearing, indicating that Dec-DISCO-cleared samples were brighter and more transparent than 3DISCO. We obtained high-quality images of the neural distributions at different depths and performed 3D reconstruction by Dec-DISCO (Fig. 3(c, d)), demonstrating higher signal intensity and better imaging quality than 3DISCO (Fig. 3(e, f)). We observed the fine neuronal

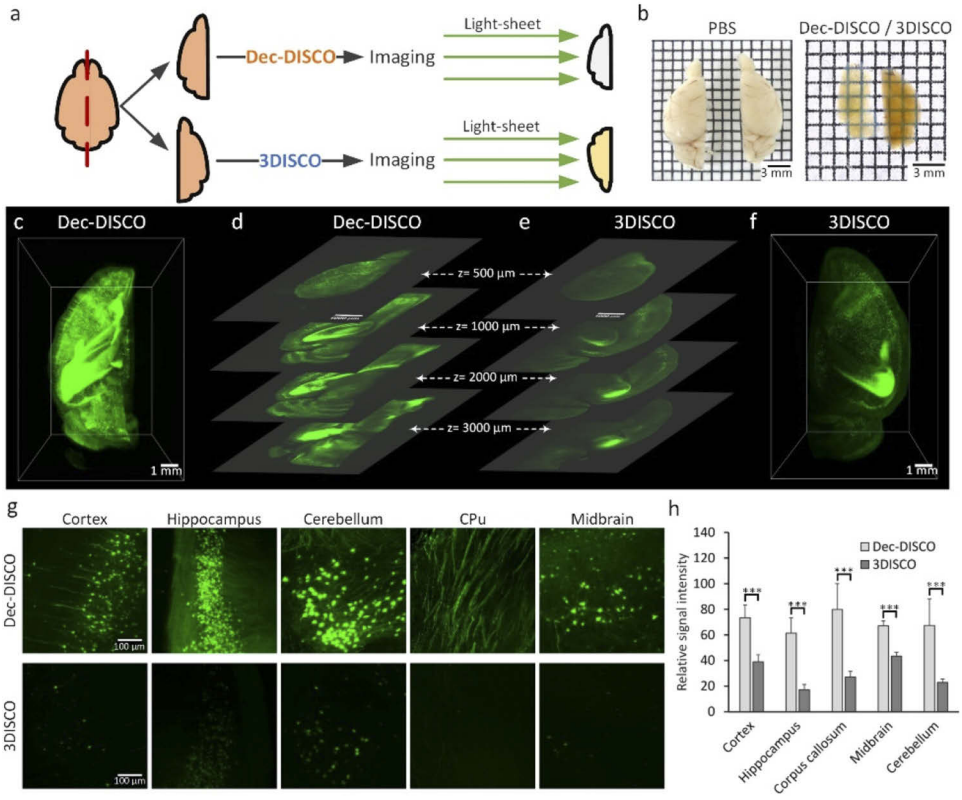

Fig. 3. Dec-DISCO is applicable for high-quality imaging of neural structures in the mouse brain using LSFM. (a) The experimental work flow. (b) Bright-field images of mouse hemispheres cleared by Dec-DISCO and 3DISCO, respectively. (c) 3D reconstruction of neural structures in the mouse hemisphere cleared by Dec-DISCO using LSFM. (d) Cross-sections of the hemisphere at different imaging depths cleared by Dec-DISCO. (e) Cross-sections of the hemisphere at different imaging depths cleared by 3DISCO. (f) 3D reconstruction of neural structures in the mouse hemisphere cleared by 3DISCO. (g) Comparison of the high-magnification images in different brain regions after Dec-DISCO and 3DISCO clearing. (h) Quantification of the fluorescence level in different brain regions after Dec-DISCO and 3DISCO. The same imaging parameters were used for imaging the brain samples cleared by Dec-DISCO and 3DISCO (n=3). All values are presented as the mean ± SD. Statistical significance in **h** (***, $P < 0.001$) was assessed by an independent-sample t-test.

Biomedical Optics EXPRESS

structures in different brain regions, including the cortex, hippocampus, cerebellum, caudate putamen (CPu), and midbrain (Fig. 3(g)). Compared with 3DISCO, Dec-DISCO treated samples revealed more neuronal details and showed a higher level of fluorescent signals in all observed regions than 3DISCO (Fig. 3(h)).

In addition, we also imaged and reconstructed the nerve branches within skeletal muscles using *Thy1*-YFP-16 transgenic mice (Fig. S5). Due to the high transparency and fluorescence enhancement, Dec-DISCO allowed fine imaging and reconstruction of nerve branches at different depths, while 3DISCO could not.

3.4. Dec-DISCO can be used to 3D image heme-rich mouse lungs labeled with quantum dots

Quantum dots are crystals of fluorescent semiconductor material with a nanoscale diameter (2–10 nm). Due to their very narrow fluorescence spectra, high brightness, and resistance to photobleaching, quantum dots have been widely used as biomarkers for molecular labeling in many biomedical studies, especially for early tumor diagnosis and treatment [38–40]. Therefore, visualization of their distribution and densities within mouse organs in 3D can provide useful information for drug delivery and tumor therapy.

Here, we injected CdSe@ZnS quantum dots intravenously into C57BL/6J mice, and the lung samples were extracted several hours after injection and post-fixed overnight, followed by Dec-DISCO/3DISCO clearing and LSFM imaging (Fig. 4(a)). As shown in Fig. 4(b), the fixed lung samples contained a large amount of residual blood, therefore the cleared samples showed a very dark red color after 3DISCO clearing. In contrast, Dec-DISCO could efficiently elute the heme within the lungs and achieved full transparency (Fig. 4(b)). Then we performed 3D imaging and reconstruction of 3DISCO/Dec-DISCO cleared mouse lungs labeled by quantum dots (Fig. 4(c, d)). The fluorescence images at different depths were shown (Fig. 4(e)-(g)). Samples cleared by Dec-DISCO could be finely imaged from the sample surface to the deep region without any blind area (Fig. 4(e, f)); however, the middle of the 3DISCO-treated samples in the deep region remained an invisible dark area due to the heavy light absorption caused by residual blood, resulting in the incomplete acquisition of fluorescent signals of the entire samples (Fig. 4(g, h)).

3.5. Dec-DISCO is applicable for visualization of neural information in injured spinal cord with hemorrhage

Spinal cord injury can lead to irreversible damage to neurons and axons, causing motor and sensory dysfunction, loss of movement, and even permanent paralysis [41]. Many studies have proved that spinal cord injury is often accompanied by serious secondary hemorrhage, further aggravating the injury [35,41]. 3DISCO method has been used for studying spinal cord injury and neural regeneration in recent publications [12,35]. However, the mass hemorrhage in the injury area of spinal cords might limit the imaging quality of 3DISCO. Here, we employed a weight-drop contusion spinal injury model using *Thy1*-GFP-M mice, and the injured spinal cords were harvested, followed by Dec-DISCO/3DISCO clearing and LSFM imaging (Fig. 5(a)). The bright-field images showed visible residual blood within the injured spinal cord, and the redness of blood in the injury area became evident after 3DISCO clearing (Fig. 5(b)). Dec-DISCO could efficiently decolorize the spinal cord and achieved better transparency than 3DISCO (Fig. 5(b)). The 3D imaging of injured spinal cords showed that 3DISCO failed to image the entire spinal cord due to the heavy residual blood, leaving most of the injury area black (Fig. 5(c)). Dec-DISCO allowed fine imaging of neural structures in the entire spinal cord (Fig. 5(d)), not only the healthy neural structures were well visualized in the normal area (Fig. 5(e)), but also the disruption of neurons and axons were observed in the injury area (Fig. 5(f)). While 3DISCO only allowed visualization of neurons in the normal area and left the injury region blind (Fig. 5(g, h)). These

Biomedical Optics EXPRESS

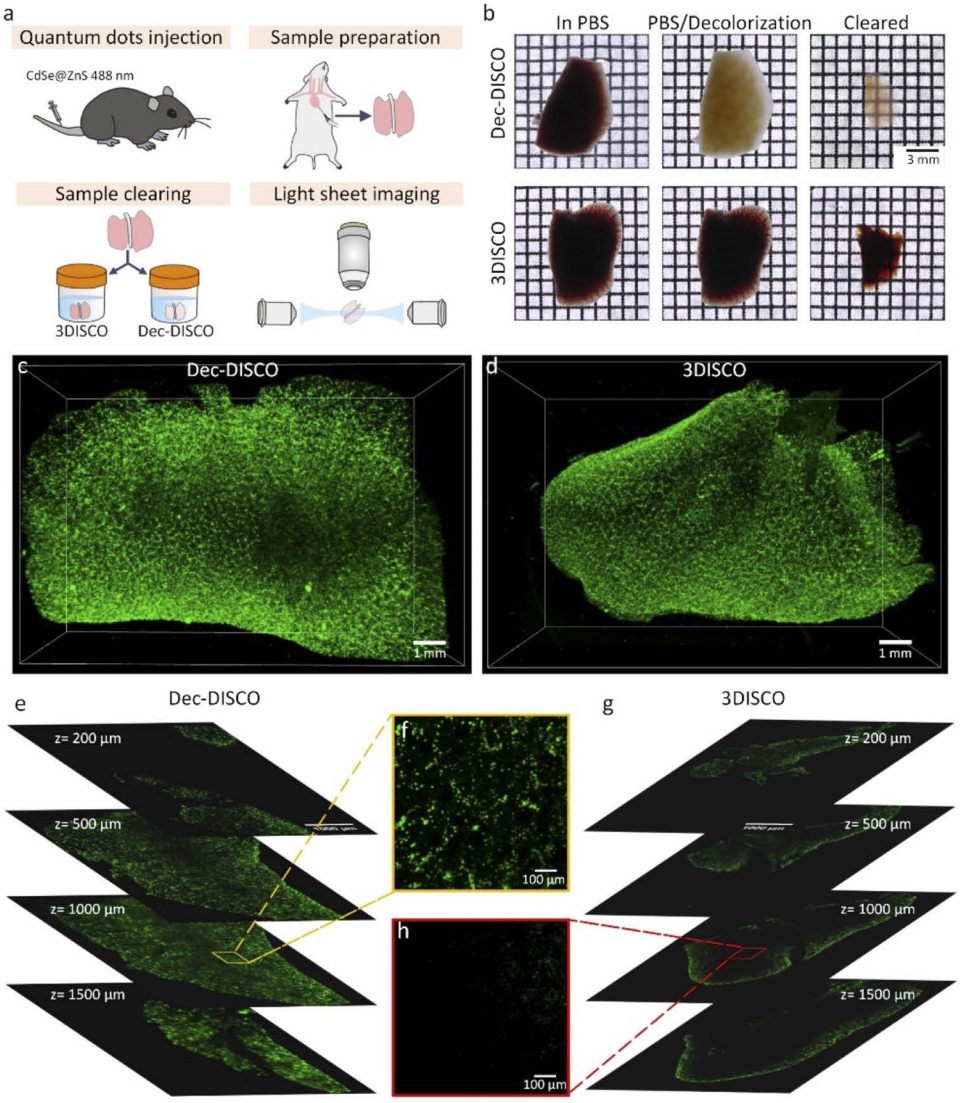

Fig. 4. Dec-DISCO achieved complete 3D imaging with no blind area for heme-rich mouse lungs labeled by quantum dots. (a) Experimental design for clearing and imaging of mouse lungs labeled by quantum dots. (b) Bright-field images of labeled mouse lungs before and after clearing with Dec-DISCO and 3DISCO, respectively. (c) 3D reconstruction of cell populations labeled by quantum dots in the mouse lungs cleared by Dec-DISCO. (d) 3D reconstruction of cell populations labeled by quantum dots in the mouse lungs cleared by 3DISCO. (e) Cross-section images of the lungs in **c** at different imaging depths. (f) Magnification of boxed regions in **e**. (g) Cross-section images of the lungs in **d** at different imaging depths. (h) Magnification of boxed regions in **g**.

Biomedical Optics EXPRESS

results suggested that Dec-DISCO is a powerful tool to promote biomedical researches related to spinal cord injury.

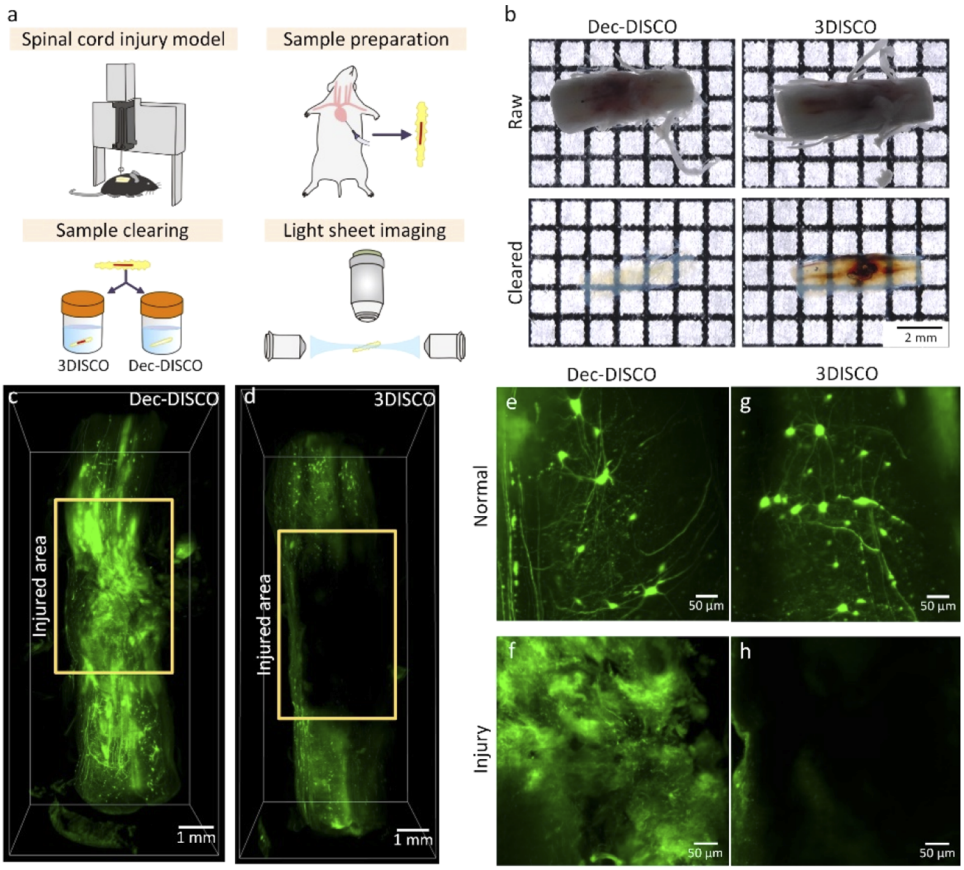

Fig. 5. Dec-DISCO permits 3D visualization of neural disruptions in injured spinal cord with severe hemorrhage. (a) Experimental design for clearing and imaging of injured spinal cords from spinal cord injury model. (b) Bright-field images of injured spinal cords before and after clearing with Dec-DISCO and 3DISCO. (c) 3D imaging of neural structures of injured spinal cord cleared by Dec-DISCO. (d) 3D imaging of neural structures of injured spinal cord cleared by 3DISCO. (e, f) Visualization of neural information in normal (e) and injured area (f) cleared by Dec-DISCO. (g, h) Visualization of neural information in normal (g) and injured area (h) cleared by 3DISCO.

4. Discussion and conclusion

In recent years, 3DISCO method has been widely used in many studies due to its superior clearing capabilities; however, the sensitivity to residual blood within tissue limited its applications in heme-rich tissue. In this study, we modified 3DISCO method by introducing an effective decolorization solution—CUBIC-L, for pretreatment of heme-rich tissue, termed Dec-DISCO. Dec-DISCO achieves more excellent transparency on many kinds of tissue and performs better fluorescence preservation than 3DISCO. Combined with LSFM, Dec-DISCO performed superior imaging quality in 3D reconstruction of neuronal structures in mouse brains. Dec-DISCO also allowed 3D imaging of heme-rich organs labeled with quantum dots and could be used to study neural disruptions in spinal cord injury with severe hemorrhage.

Biomedical Optics EXPRESS

Decolorization solution is very critical for optimizing 3DISCO method. Traditional reagents such as H_2O_2 and NaOH are often used for tissue decolorization in previous studies [13,25]. Recently, several effective chemical solutions were discovered, showing good decolorizing capability, including SDS [27], CUBIC-R1 [24], and CUBIC-L [26]. We found that CUBIC-L was not only effective for tissue decolorization but also notably increased the signal intensities of endogenous GFP fluorescence, which was not achieved by any other tested solutions. This may be due to the chemical nature of N-butyldiethanolamine used in CUBIC-L, for example, its alkaline condition in water. The feature of fluorescence enhancement can effectively make up for the quenching of fluorescence by 3DISCO. More importantly, Dec-DISCO protocol also showed much better fluorescence preservation than original CUBIC protocol after complete clearing, making Dec-DISCO more powerful in imaging transgenic mouse tissue. It should be noted that this modification strategy by introducing CUBIC-L for decolorization prior to clearing should be effective for other solvent-based clearing protocols, such as FDISCO, which did not take decolorization into consideration [15]. The combination of this decolorization step with FDISCO is expected to achieve higher transparency and more enhanced fluorescence intensity.

Quantum dots can easily label cells with no interference with cell functionality or migration capacities, thus they are widely used for many biomedical studies, especially for early tumor diagnosis and treatment [38–40]. However, when applied to heme-rich tissue such as lungs, though careful intracardial perfusion with PBS was done prior to tissue extraction, a large amount of residual blood was still retained, which will significantly affect the sample transparency and imaging quality. Dec-DISCO is successfully applied to 3D imaging of lungs labeled by quantum dots, which may benefit studies related to cancer diagnosis and targeted therapy.

Several diseases induced by external force will cause traumatic injuries and severe hemorrhage within tissue, such as spinal cord injury [37,41]. 3DISCO method was developed to study axon regeneration after spinal cord injury; however, when faced with hemorrhage, 3DISCO could not deal with the blood within tissue. Dec-DISCO efficiently eluted the residual blood within injured spinal cord, thus successfully revealed the disruption of neurons and axons in the injured area, while 3DISCO could not.

Tissue shrinkage can hardly be avoided in solvent-based clearing methods. This overall reduction in tissue size offers advantages for the visualization of large tissue. However, extensive tissue shrinkage may also cause damage to the structural integrity of tissue, which may disturb morphological analyses after clearing. Though the shrinkage caused by Dec-DISCO is proved to be uniform on brain slices, the increased tissue shrinkage still brings risks for tissue deformation. Therefore, tissue shrinkage still needs to be carefully validated in future studies.

It should be noted that current aqueous-based tissue clearing methods also play an important role in the tissue clearing field, such as CUBIC [1]. CUBIC-series methods enable high-performance clearing of mouse brains and organs; however, it may be time-consuming when applied CUBIC to large tissues such as rat organs, largely due to the long time needed for complete delipidation by CUBIC-L [42]. Dec-DISCO protocol employed CUBIC-L only for decolorization rather than delipidation, and the clearing was achieved by efficient dehydration/delipidation by tetrahydrofuran and RI matching by DBE, thus achieving better transparency in a shorter time than CUBIC on large tissues. Though Dec-DISCO has certain advantages over CUBIC, choosing a proper clearing method depends largely on specific experimental needs. In some cases, the users may prefer solvent-based clearing methods if they require shorter clearing time, better transparency, and hardening of the cleared tissues. The final goal of this study is to provide an effective protocol to solve the blood sensitivity problems raised by the solvent-based 3DISCO method which has been widely used in numerous studies. We widen the application of 3DISCO method into heme-rich tissues by introducing effective decolorization reagents proposed by CUBIC. This successful combination of the two methods facilitates the communication between

Biomedical Optics EXPRESS

the two kinds of approaches and may further provide useful information for developing new clearing methods.

Additionally, several newly-developed clearing methods based on organic solvents also introduced decolorization steps, such as PEGASOS [18] and vDISCO [16]. PEGASOS performs nicely on both hard bones and soft organs [18]. vDISCO has done beautiful works on demonstrating the applications of imaging TBI-induced injury of the PNS [16]. However, both of them used Quadrol or Quadrol-based CUBIC-R1 reagents for tissue decolorization. As shown in this work, CUBIC-L performed better than Quadrol and CUBIC-R1, especially for enhanced fluorescence signals. This allows Dec-DISCO to perform well not only for clearing but also for fluorescence preservation. Therefore, Dec-DISCO may not need extra steps such as nanoboosting to enhance the fluorescence signal. Given 3DISCO has been recognized as a pioneer clearing method for 3D imaging of transgenic-labeled or immunolabeled samples [13,31,33], this Dec-DISCO protocol is expected to further expand the applications of 3DISCO into surgical animal disease models with accurate injury and hemorrhage, as well as hold great potential for clinical examination of pathological tissue in various medical conditions, such as serious injury, tumors and cancer therapy.

In conclusion, we believe this optimized Dec-DISCO protocol will provide an efficient and powerful complement for clearing and imaging of heme-rich tissues and is expected to be used for studying various pathological diseases.

Funding. National Key Research and Development Program of China (2017YFA0700501); National Natural Science Foundation of China (61860206009, 81870934, 81961138015, 91749209); China Postdoctoral Science Foundation (2021M691145, BX20200138); the Innovation Fund of WNLO.

Acknowledgment. The authors thank Yuandi Zhao for help with the fluorescent quantum dots labeling. The authors also thank the Optical Bio-imaging Core Facility of WNLO-HUST for support with data acquisition.

Disclosures. The authors declare no conflicts of interest.

Data availability. Data underlying the results presented in this paper are not publicly available at this time but may be obtained from the authors upon reasonable request.

Supplemental document. See Supplement 1 for supporting content.

References

1. H. R. Ueda, A. Erturk, K. Chung, V. Gradinaru, A. Chedotal, P. Tomancak, and P. J. Keller, "Tissue clearing and its applications in neuroscience," Nat. Rev. Neurosci. **21**(2), 61–79 (2020).
2. S. Zhao, M. I. Todorov, R. Cai, R. A. Maskari, H. Steinke, E. Kemter, H. Mai, Z. Rong, M. Warmer, K. Stanic, O. Schoppe, J. C. Paetzold, B. Gesierich, M. N. Wong, T. B. Huber, M. Duering, O. T. Bruns, B. Menze, J. Lipfert, V. G. Puelles, E. Wolf, I. Bechmann, and A. Erturk, "Cellular and Molecular Probing of Intact Human Organs," Cell **180**(4), 796–812.e19 (2020).
3. T. Yu, Y. Qi, H. Gong, Q. Luo, and D. Zhu, "Optical clearing for multiscale biological tissues," J. Biophotonics **11**(2), e201700187 (2018).
4. I. Costantini, R. Cicchi, L. Silvestri, F. Vanzi, and F. S. Pavone, "In-vivo and ex-vivo optical clearing methods for biological tissues: review," Biomed. Opt. Express **10**(10), 5251–5267 (2019).
5. D. Zhu, K. V. Larin, Q. Luo, and V. V. Tuchin, "Recent progress in tissue optical clearing," Laser Photonics Rev. **7**(5), 732–757 (2013).
6. H. M. Lai, W. L. Ng, S. M. Gentleman, and W. Wu, "Chemical probes for visualizing intact animal and human brain tissue," Cell Chem. Biol. **24**(6), 659–672 (2017).
7. V. Marx, "Optimizing probes to image cleared tissue," Nat. Methods **13**(3), 205–209 (2016).
8. V. V. Tuchin, I. L. Maksimova, D. Zimnyakov, I. L. Kon, A. H. Mavlyutov, and A. A. Mishin, "Light propagation in tissues with controlled optical properties," J. Biomed. Opt. **2**(4), 401–417 (1997).
9. D. S. Richardson and J. W. Lichtman, "Clarifying tissue clearing," Cell **162**(2), 246–257 (2015).
10. K. Tainaka, A. Kuno, S. I. Kubota, T. Murakami, and H. R. Ueda, "Chemical principles in tissue clearing and staining protocols for whole-body cell profiling," Annu. Rev. Cell Dev. Biol. **32**(1), 713–741 (2016).
11. A. Erturk, K. Becker, N. Jahrling, C. P. Mauch, C. D. Hojer, J. G. Egen, F. Hellal, F. Bradke, M. Sheng, and H. U. Dodt, "Three-dimensional imaging of solvent-cleared organs using 3DISCO," Nat. Protoc. **7**(11), 1983–1995 (2012).
12. A. Erturk, C. P. Mauch, F. Hellal, F. Forstner, T. Keck, K. Becker, N. Jahrling, H. Steffens, M. Richter, M. Hubener, E. Kramer, F. Kirchhoff, H. U. Dodt, and F. Bradke, "Three-dimensional imaging of the unsectioned adult spinal cord to assess axon regeneration and glial responses after injury," Nat. Med. **18**(1), 166–171 (2012).

Biomedical Optics EXPRESS

13. N. Renier, Z. Wu, D. J. Simon, J. Yang, P. Ariel, and M. Tessier-Lavigne, "iDISCO: a simple, rapid method to immunolabel large tissue samples for volume imaging," Cell **159**(4), 896–910 (2014).
14. C. Pan, R. Cai, F. P. Quacquarelli, A. Ghasemigharagoz, A. Lourbopoulos, P. Matryba, N. Plesnila, M. Dichgans, F. Hellal, and A. Erturk, "Shrinkage-mediated imaging of entire organs and organisms using uDISCO," Nat. Methods **13**(10), 859–867 (2016).
15. Y. Qi, T. Yu, J. Xu, P. Wan, Y. Ma, J. Zhu, Y. Li, H. Gong, Q. Luo, and D. Zhu, "FDISCO: advanced solvent-based clearing method for imaging whole organs," Sci. Adv. **5**(1), eaau8355 (2019).
16. R. Cai, C. Pan, A. Ghasemigharagoz, M. I. Todorov, B. Förstera, S. Zhao, H. S. Bhatia, A. Parra-Damas, L. Mrowka, D. Theodorou, M. Rempfler, A. L. R. Xavier, B. T. Kress, C. Benakis, H. Steinke, S. Liebscher, I. Bechmann, A. Liesz, B. Menze, M. Kerschensteiner, M. Nedergaard, and A. Ertürk, "Panoptic imaging of transparent mice reveals whole-body neuronal projections and skull–meninges connections," Nat. Neurosci. **22**(2), 317–327 (2019).
17. C. Hahn, K. Becker, S. Saghafi, M. Pende, A. Avdibašić, M. Foroughipour, D. E. Heinz, C. T. Wotjak, and H.-U. Dodt, "High-resolution imaging of fluorescent whole mouse brains using stabilised organic media (sDISCO)," J. Biophotonics **12**(8), e201800368 (2019).
18. D. Jing, S. Zhang, W. Luo, X. Gao, Y. Men, C. Ma, X. Liu, Y. Yi, A. Bugde, B. O. Zhou, Z. Zhao, Q. Yuan, J. Q. Feng, L. Gao, W.-P. Ge, and H. Zhao, "Tissue clearing of both hard and soft tissue organs with the PEGASOS method," Cell Res. **28**(8), 803–818 (2018).
19. M. T. Ke, Y. Nakai, S. Fujimoto, R. Takayama, S. Yoshida, T. S. Kitajima, M. Sato, and T. Imai, "Super-resolution mapping of neuronal circuitry with an index-optimized clearing agent," Cell Rep. **14**(11), 2718–2732 (2016).
20. M. T. Ke, S. Fujimoto, and T. Imai, "SeeDB: a simple and morphology-preserving optical clearing agent for neuronal circuit reconstruction," Nat. Neurosci. **16**(8), 1154–1161 (2013).
21. H. Hama, H. Hioki, K. Namiki, T. Hoshida, H. Kurokawa, F. Ishidate, T. Kaneko, T. Akagi, T. Saito, T. Saido, and A. Miyawaki, "ScaleS: an optical clearing palette for biological imaging," Nat. Neurosci. **18**(10), 1518–1529 (2015).
22. X. Zhu, L. Huang, Y. Zheng, Y. Song, Q. Xu, J. Wang, K. Si, S. Duan, and W. Gong, "Ultrafast optical clearing method for three-dimensional imaging with cellular resolution," Proc. Natl. Acad. Sci. U. S. A. **116**(23), 11480–11489 (2019).
23. J. Zhu, T. Yu, Y. Li, J. Xu, Y. Qi, Y. Yao, Y. Ma, P. Wan, Z. Chen, X. Li, H. Gong, Q. Luo, and D. Zhu, "MACS: rapid aqueous clearing system for 3D mapping of intact organs," Adv. Sci. **7**(8), 1903185 (2020).
24. E. A. Susaki, K. Tainaka, D. Perrin, F. Kishino, T. Tawara, T. M. Watanabe, C. Yokoyama, H. Onoe, M. Eguchi, S. Yamaguchi, T. Abe, H. Kiyonari, Y. Shimizu, A. Miyawaki, H. Yokota, and H. R. Ueda, "Whole-brain imaging with single-cell resolution using chemical cocktails and computational analysis," Cell **157**(3), 726–739 (2014).
25. K. Tainaka, S. I. Kubota, T. Q. Suyama, E. A. Susaki, D. Perrin, M. Ukai-Tadenuma, H. Ukai, and H. R. Ueda, "Whole-body imaging with single-cell resolution by tissue decolorization," Cell **159**(4), 911–924 (2014).
26. K. Tainaka, T. C. Murakami, E. A. Susaki, C. Shimizu, R. Saito, K. Takahashi, A. Hayashi-Takagi, H. Sekiya, Y. Arima, S. Nojima, M. Ikemura, T. Ushiku, Y. Shimizu, M. Murakami, K. F. Tanaka, M. Iino, H. Kasai, T. Sasaoka, K. Kobayashi, K. Miyazono, E. Morii, T. Isa, M. Fukayama, A. Kakita, and H. R. Ueda, "Chemical landscape for tissue clearing based on hydrophilic reagents," Cell Rep. **24**(8), 2196–2210.e9 (2018).
27. K. Chung, J. Wallace, S. Y. Kim, S. Kalyanasundaram, A. S. Andalman, T. J. Davidson, J. J. Mirzabekov, K. A. Zalocusky, J. Mattis, A. K. Denisin, S. Pak, H. Bernstein, C. Ramakrishnan, L. Grosenick, V. Gradinaru, and K. Deisseroth, "Structural and molecular interrogation of intact biological systems," Nature **497**(7449), 332–337 (2013).
28. R. Tomer, L. Ye, B. Hsueh, and K. Deisseroth, "Advanced CLARITY for rapid and high-resolution imaging of intact tissues," Nat. Protoc. **9**(7), 1682–1697 (2014).
29. B. Yang, J. B. Treweek, R. P. Kulkarni, B. E. Deverman, C. K. Chen, E. Lubeck, S. Shah, L. Cai, and V. Gradinaru, "Single-cell phenotyping within transparent intact tissue through whole-body clearing," Cell **158**(4), 945–958 (2014).
30. Y. G. Park, C. H. Sohn, R. Chen, M. McCue, D. H. Yun, G. T. Drummond, T. Ku, N. B. Evans, H. C. Oak, W. Trieu, H. Choi, X. Jin, V. Lilascharoen, J. Wang, M. C. Truttmann, H. W. Qi, H. L. Ploegh, T. R. Golub, S.-C. Chen, M. P. Frosch, H. J. Kulik, B. K. Lim, and K. Chung, "Protection of tissue physicochemical properties using polyfunctional crosslinkers," Nat. Biotechnol. **37**(1), 73–83 (2019).
31. M. Belle, D. Godefroy, C. Dominici, C. Heitz-Marchaland, P. Zelina, F. Hellal, F. Bradke, and A. Chedotal, "A simple method for 3D analysis of immunolabeled axonal tracts in a transparent nervous system," Cell Rep. **9**(4), 1191–1201 (2014).
32. X. Yin, T. Yu, B. Chen, J. Xu, W. Chen, Y. Qi, P. Zhang, Y. Li, Y. Kou, Y. Ma, N. Han, P. Wan, Q. Luo, D. Zhu, and B. Jiang, "Spatial distribution of motor endplates and its adaptive change in skeletal muscle," Theranostics **9**(3), 734–746 (2019).
33. M. Belle, D. Godefroy, G. Couly, S. A. Malone, F. Collier, P. Giacobini, and A. Chedotal, "Tridimensional visualization and analysis of early human development," Cell **169**(1), 161–173.e12 (2017).
34. C. Soderblom, D. H. Lee, A. Dawood, M. Carballosa, A. Jimena Santamaria, F. D. Benavides, S. Jergova, R. M. Grumbles, C. K. Thomas, K. K. Park, J. D. Guest, V. P. Lemmon, J. K. Lee, and P. Tsoulfas, "3D imaging of axons in transparent spinal cords from rodents and nonhuman primates," eNeuro **2**(2), ENEURO.0001-15.2015 (2015).
35. E. R. Bray, M. Noga, K. Thakor, Y. Wang, V. P. Lemmon, K. K. Park, and P. Tsoulfas, "3D visualization of individual regenerating retinal ganglion cell axons reveals surprisingly complex growth paths," eNeuro **4**(4), ENEURO.0093-17.2017 (2017).

Biomedical Optics EXPRESS

36. J. Xu, Y. Ma, T. Yu, and D. Zhu, "Quantitative assessment of optical clearing methods in various intact mouse organs," J. Biophotonics **12**(2), e201800134 (2019).
37. Y. Yao, J. Xu, T. Yu, Z. Chen, Z. Xiao, J. Wang, Y. Hu, Y. Wu, and D. Zhu, "Flufenamic acid inhibits secondary hemorrhage and BSCB disruption after spinal cord injury," Theranostics **8**(15), 4181–4198 (2018).
38. C. Li, X. Q. Yang, M. Z. Zhang, Y. Y. Song, K. Cheng, J. An, X. S. Zhang, Y. Xuan, B. Liu, and Y. D. Zhao, "In vivo imaging-guided nanoplatform for tumor targeting delivery and combined chemo-, gene- and photothermal therapy," Theranostics **8**(20), 5662–5675 (2018).
39. Y. Y. Song, C. Li, X. Q. Yang, J. An, K. Cheng, Y. Xuan, X. M. Shi, M. J. Gao, X. L. Song, Y. D. Zhao, and W. Chen, "Graphene oxide coating core-shell silver sulfide@mesoporous silica for active targeted dual-mode imaging and chemo-photothermal synergistic therapy against tumors," J. Mater. Chem. B **6**(29), 4808–4820 (2018).
40. X. Michalet, F. F. Pinaud, L. A. Bentolila, J. M. Tsay, S. Doose, J. J. Li, G. Sundaresan, A. M. Wu, S. S. Gambhir, and S. Weiss, "Quantum dots for live cells, in vivo imaging, and diagnostics," Science **307**(5709), 538–544 (2005).
41. V. Gerzanich, S. K. Woo, R. Vennekens, O. Tsymbalyuk, S. Ivanova, A. Ivanov, Z. Geng, Z. Chen, B. Nilius, V. Flockerzi, M. Freichel, and J. M. Simard, "De novo expression of Trpm4 initiates secondary hemorrhage in spinal cord injury," Nat. Med. **15**(2), 185–191 (2009).
42. K. Matsumoto, T. T. Mitani, S. A. Horiguchi, J. Kaneshiro, T. C. Murakami, T. Mano, H. Fujishima, A. Konno, T. M. Watanabe, H. Hirai, and H. R. Ueda, "Advanced CUBIC tissue clearing for whole-organ cell profiling," Nat. Protoc. **14**(12), 3506–3537 (2019).